

TESTING OF ELECTRODES FOR HIGH TEMPERATURE
SOLID ELECTROLYTE FUEL CELLS

E. F. Sverdrup, D. H. Archer, J. J. Alles, and A. D. Glasser

Westinghouse Research Laboratories
Beulah Road, Churchill Borough
Pittsburgh 35, Pennsylvania

INTRODUCTION

Fuel cell systems utilizing zirconium dioxide ceramic electrolytes are being developed both for electric power generation and for the electrolytic regeneration of oxygen from carbon dioxide-water vapor mixtures. Practical devices operate at temperatures in the vicinity of 1000°C in order to obtain high oxygen ion mobility in the electrolyte material. The measurement of the energy losses associated with electrode operation in air and fuel atmospheres under these high temperature conditions is the subject of this paper.

ELECTRODE PROCESSES IN THE SOLID ELECTROLYTE FUEL CELLS

A typical solid electrolyte fuel cell battery is shown in Fig. 1. It consists of a series of bell-and-spigot shaped cells which nest together to form a tube. A fuel stream is passed through the inside of the tube and air surrounds the outside. The steps involved in the reaction of the fuel and oxidant to produce reaction products and electric power can be visualized with the aid of Fig. 2. Oxygen molecules diffuse through the air to the air electrode surface where they dissociate and are adsorbed. Surface migration occurs over the electrode to sites at the electrode-electrolyte interfaces where, combining with two electrons from the electrodes, an oxygen atom becomes an O^{2-} ion and enters an oxygen ion vacancy in the crystal lattice of the electrolyte. Oxygen ion transport through the electrolyte occurs. At the fuel electrode, oxygen ions leave the electrolyte give up electrons to the electrode and react with fuel species which have diffused to and been adsorbed on the fuel electrode surface. The products of the surface-reaction with the fuel are desorbed from the electrode and diffuse into the fuel reaction-product stream. The electrons that have been delivered to the fuel electrode pass through the conducting seal to the air electrode of the next cell where they again take part in the formation of oxygen ions. At the terminals of each cell a generated voltage appears (if the external electric circuit is open) which is given by:

$$E_g = \frac{RT}{4F} \ln \frac{P_{O_2H}}{P_{O_2L}}$$

E_g = open circuit voltage of the cell (volts)

R = gas constant, 8.134 (joules/°K-mole)

T = absolute temperature (°K)

F = Faraday number (96,500 coul/gm. equiv.)

P_{O_2H} = oxygen partial pressure at the air electrode of the cell

P_{O_2L} = oxygen partial pressure on the fuel electrode of the cell

This voltage reflects the reversible energy available from the isothermal expansion of an ideal gas between the two oxygen partial pressure levels. If the circuit is closed so that electric power is delivered to an external load, the voltage V_T appearing at the terminals of the cell is decreased by irreversible losses. If the battery operates at a load current I equal to the reaction of \dot{n}_{O_2}

moles of O_2 per second ($I = 4F \dot{n}_{O_2} \frac{\text{coulombs}}{\text{mole } O_2} \times \frac{\text{mole } O_2}{\text{sec}}$), then the

cell terminal voltage is decreased both by the ohmic resistance losses caused by the transport of electrons through the electrodes and $O^=$ ions through the electrolyte and by the irreversible losses associated with the transport of reactants and reaction products to and from the electrodes. Irreversible losses associated with the adsorption, desorption and surface reaction steps may also occur.

$$V_T = E_g - IR - V_p$$

V_T = terminal voltage of the cell (volts)

E_g = generated, open circuit, voltage of the cell (volts)

I = cell current (amperes)

R = total ohmic resistance between cell terminals, electrodes and electrolyte (ohms)

V_p = total voltage loss due to non-ohmic irreversible processes (volts)

The ohmic resistance loss "R" may be conveniently separated into components due to electron transport in the air electrode, the air electrode-to-electrolyte contact resistance, the ionic resistance of the electrolyte, the fuel electrode-to-electrolyte contact resistance, and the electronic resistance of the fuel electrode. Techniques have been developed for isolating and measuring these separately. The polarization voltage losses are not as easily separated but the overall potential loss associated with carrying out either the fuel or air electrode reaction can be measured as a function of the reaction rate (electrode current density) by measuring the non-ohmic potential drop between the appropriate electrode and the electrolyte.

AN APPARATUS FOR THE MEASUREMENT OF ELECTRODE LOSSES

Figure 3 is a schematic of an apparatus for measuring electrode losses. It consists of a furnace, a gas-tight system for reactant delivery and removal, and a number of spring-loaded probes

which bear on an electroded test sample. Each probe is a Pt-Pt 10% Rh thermocouple which can be used for sensing temperatures as well as potential. Fig. 4 is a photograph of the test cavity showing the probe arrangement. An electroded test wafer rests in the cavity and probes bear on both the upper and lower surfaces of the test specimen when the tester is assembled.

The probe arrangement shown in Fig. 4 and again in Fig. 5 allows a number of tests to be made. As can be seen from Fig. 5, the test sample is a wafer of the ceramic electrolyte with the electrode to be tested applied to one surface and a suitable counter electrode to the other surface. The electrode is applied as a band leaving a portion of the bare electrolyte surface exposed. Five probes bear on the electroded portion of each surface while the sixth probe rests on the electrolyte surface.

This choice of electrode and electrolyte probe locations allows the important electrode characteristics to be measured. The techniques involved are described in succeeding sections.

MEASUREMENT OF THE OHMIC LOSSES ASSOCIATED WITH ELECTRON TRANSPORT IN THE ELECTRODE

The losses which are associated with the transport of electrons along the electrode film to the sites where oxygen ions are formed depend on the electronic resistivity of the electrode material and on the geometry of the electrode. Expressions which take into account the non-uniform current density distribution in the electrode are easily derived but are less useful than the simplified approximation:

$$R_{\text{electrode}} = \frac{\rho_e}{\delta_e} \frac{\bar{l}_e}{\pi D}$$

where

ρ_e = electronic resistivity of the electrode material (ohm-cm)

\bar{l}_e = effective length of electron travel along electrode (cm)

δ_e = electrode thickness (cm)

πD = circumference of fuel cell (width of electrode) (cm)

As this expression shows, the parameter of interest to the fuel cell designer is the electrode resistivity divided by the electrode film thickness " ρ_e/δ_e ". This quantity is easily measured in the electrode tester by passing a current between two of the probes bearing on the electrode and measuring, potentiometrically, the potential drop across two other electrode potential probes. Solution of the two dimensional current flow problem for the geometry used allows the direct determination of ρ_e/δ_e from the measured ratio of voltage to current flow. Alternatively, the treatment of the potential problem by L. J. van der Pauw¹ allows ρ_e/δ_e to be calculated from measurements using four probes placed arbitrarily on the edges of an electrode film of arbitrary shape. The required measurements are indicated in Fig. 6. The two voltage-to-current ratios yield directly a value of the resistivity/thickness of the electrode film. In addition, the use of two differing current paths in the measurements allows major changes in the uniformity of the film during electrode operation to be easily detected. As an example of

these measurements, Fig. 7 compares the temperature dependence of a porous sintered platinum electrode and a fused platinum film electrode, as determined by the van der Pauw technique, with the calculated temperature variation of a sheet of bulk platinum having the same weight density. As would be expected from the character of the cross-sections of these films, shown in Fig. 8, the sintered electrode displays a ρ_e/δ_e about three times that of bulk platinum. The fused electrode film shows ρ_e/δ_e values about 1.5 times greater than bulk platinum. This increased effective resistivity gives some indication of the microporosity of the electrode film. Figure 7 also shows the irreversible increases in resistivity/thickness parameter displayed by both types of electrode when exposed to hydrogen-water atmospheres.

MEASUREMENT AND SEPARATION OF ELECTRODE TO ELECTROLYTE LOSSES

The voltage losses associated with the operation of an electrode are measured using the electrode tester by passing a current through the (electrode)-(electrolyte)-(counter-electrode) test wafer and measuring the voltage drop between two non-current carrying potential probes - one bearing on the test electrode and the other on the bare electrolyte. In practice current is introduced through the four probes located at the corners of the electrode and the potential is monitored between the center electrode probe and the electrolyte probe. The electrolyte probe, as shown in Fig. 5, is located as far as possible from the edge of the electrode. The direction of current flow determines the direction of oxygen ion transport and the reactions which take place at the test electrode. By appropriate choice of current direction and atmosphere either the air or the fuel electrode processes may be studied as illustrated in Fig. 9.

A Tektronix type 545 oscilloscope with a type D high gain differential input-d.c. amplifier is used to monitor the potential drop from the electrode to the electrolyte. The differential input rejects noise voltages common to both leads of the measuring circuit. The single trace mode of sweep operation is used and the gate output, a d.c. voltage of 30 volts which becomes available at the front panel of the scope when the sweep is initiated, is used in conjunction with a booster battery and a fast relay* to energize or de-energize the electrode current circuit. (Fig. 10) Oscilloscope traces such as are shown in Fig. 11 are obtained.

When the relay closes establishing current through the sample the electrode to electrolyte voltage rises to an intermediate value so rapidly that no trace can be detected on the oscillogram and then rises at a slower rate until the steady state potential drop corresponding to the given electrode current density is reached.

*C. P. Clare, Model HG 1202 - operating time 5 milliseconds with 52.5 volts step function voltage applied to the coil.

Similarly, when the relay opens, the potential decays almost immediately to an intermediate level and then more slowly to zero. The fast processes, which occur so rapidly that no trace is recorded on the oscillogram, are associated primarily with the resistive voltage drop occasioned by the passage of oxygen ions through the electrolyte. This can be seen by comparison of the magnitudes of the fast component of the potential drop with predictions of the electrolyte resistance based on the known resistivity of the electrolyte and the geometry of the sample. The strong temperature dependence of the electrolyte resistivity offers a convenient method of separating electrolyte resistance from other possible rapid polarization processes which would be expected to show a different temperature dependence.

An illustrative set of current interruption photographs taken on a fused-electrode test sample operating in oxygen at 900°C are shown in Fig. 12. The fast component of the total voltage drop across the specimen, V_{4-10} , can be scaled from the current interruption photographs and is 680 millivolts. Under the conditions of this test, a sample current of 1000 milliamps was being passed through the specimen. An overall "resistance" of 680 mv/1000 ma = 0.68 ohms is indicated. At 900°C the resistivity of $(ZrO_2)_{0.9}(Y_2O_3)_{0.1}$ electrolyte materials is 12 ohm-cm. The sample resistance calculated from geometry is then:

$$R_{4-10} = \frac{\rho_b \delta_b}{A} = \frac{12 (\Omega - \text{cm}) 0.09 (\text{cm})}{1.36 (\text{sq. cm})} = 0.80 \Omega \quad (1)$$

where ρ_b = electrolyte resistivity (ohm-cm)

δ_b = electrolyte thickness (cm)

A = electrode area (sq. cm)

The measured resistance is 85% of the resistance estimated from sample geometry. Measurements of total sample resistance were made at various temperatures between 800°C and 1000°C. The results are plotted in Fig. 13 and compared with calculated values based on sample geometry. As is evident from Fig. 13, the temperature dependence of the sample resistance is the same as that of the electrolyte, the total sample resistance remaining 85% of the calculated except at the lowest temperature - 800°C.

The accuracy with which electrode area can be measured is probably ±5% and the electrolyte resistance is known only to ±5%, so the agreement between the magnitude of the resistance characterizing the "fast process" polarization and the ohmic resistance of the electrolyte seems satisfactory.

MEASUREMENT OF THE ELECTRICAL POSITION OF THE ELECTROLYTE POTENTIAL PROBE

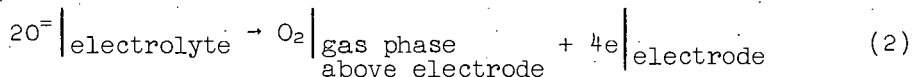
Figs. 12 and 13 illustrate the method used for establishing the electrical position of the electrolyte potential probe. If the electrolyte probe were positioned away from the edge of the electrode, at a distance which is large compared to the spacing between electrodes,

the ohmic resistance of the electrolyte included in measurement between electrode and probe would approach one half the total electrolyte resistance of the sample. In practice, it is difficult to achieve a separation between electrode and probe of more than twice the electrolyte thicknesses. It is also difficult to control the position of the probe with respect to the edge of the electrode. As a consequence, the electrical position of the probe does not usually fall in the center of the electrolyte. As Fig. 2 shows, in Test XXXII the probe was positioned electrically closer to the fused test electrode, the ratio of the resistance between this electrode and probe (R_{4-7}) and the total resistance (R_{4-10}) being $0.19/0.68 = 0.28$. Figure 12 demonstrates that this ratio remained constant, independent of test temperature and atmosphere.

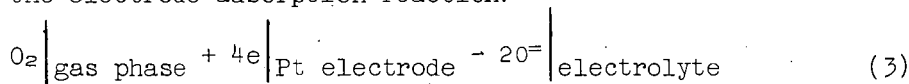
MEASUREMENT OF "SLOW" POLARIZATION PROCESSES

Figure 14 illustrates the usefulness of the current interruption technique in the investigation of electrode polarization. Here the polarization voltages of a particular electrode in oxygen and hydrogen-water atmosphere are compared. The electrode displays low polarization voltage losses when tested in oxygen atmospheres. In fuel atmospheres, large polarization losses, which decay on interruption of the current in times of the order 10 to 100 milliseconds, are typical. Volt-ampere characteristics of the electrode sample constructed from current interruption data taken in pure oxygen (Fig. 15) and in hydrogen (Fig. 16) are shown.

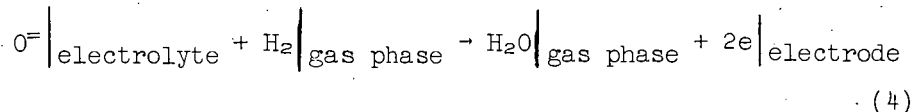
Evidently, the electrode desorption reaction:



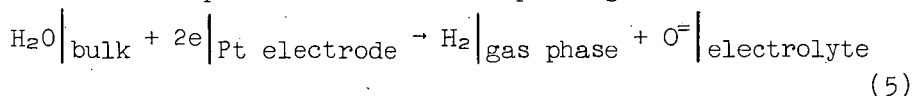
and the electrode adsorption reaction:



which take place in oxygen atmospheres are very nearly reversible even at current densities up to 750 ma/cm^2 . In fuel atmospheres the overall desorption reaction corresponding to reaction (2) is:



The overall adsorption reaction corresponding to reaction (3) is:



These reactions are not reversible at even moderate current densities. The degree of irreversibility corresponding to various current densities (i.e., reaction rates) has been measured over a range from zero to 750 ma/cm² and over the temperature range 1000°C to 750°C. The results of these tests are presented in Fig. 17.

Current interruption techniques have been used by others² to study the polarization behavior of molten carbonate cells at 600°C. Polarizations of 0.3 - 0.6 volt at current densities of 100 ma/cm² having decay times of over one second are observed at the hydrogen electrode. At the air electrode, polarizations of about 0.09 volts, with decay times between 10⁻² and 10⁻¹ seconds, are reported. These results may be compared with those presented in Figs. 14-17 which show hydrogen electrode polarizations of 0.05 volts with decay times of about 10⁻¹ seconds at 100 ma/cm². Air electrode polarizations are less than 10 mv and decay is less than 10⁻³ seconds.

ADDITIONAL CONSIDERATIONS IN THE INTERPRETATION OF ELECTRODE TESTER RESULTS HEATING EFFECTS ON THE SAMPLE CURRENT

Comparison of the current establishment and current interruption oscillograms of Fig. 11 shows that the current establishment oscillogram displays a resistive component of $\frac{500 \text{ mv}}{1450 \text{ ma}} = 0.34 \Omega$ while the current interruption photograph indicates a lowered resistive component of $\frac{400 \text{ mv}}{1450 \text{ ma}} = 0.28 \Omega$.

Measurements at other current levels indicate that the resistive voltage drop as measured from the current establishment photographs is directly proportional to current. Resistive drops measured from current interruption photographs depart from linearity at high electrode current densities. This difference may be attributed to heating of the sample by the passage of current. The strong temperature dependence of electrolyte resistivity causes appreciable changes in the sample resistance. Because polarization may also be strongly temperature dependent; this heating effect must be taken into account in obtaining polarization data such as is shown in Fig. 17. Since the sample is in thermal equilibrium with the tester furnace when current establishment oscillograms are taken, these oscillograms may be used to indicate the true resistance corresponding to the known sample temperatures. The major polarizations require times comparable to the thermal time constants of the system to reach equilibrium, hence their measurement from current-make oscillograms is not accurate. Current break oscillograms which yield the polarization corresponding to steady-state operation of the electrode at a given current density are more reliable. An estimate of the electrode operating temperature corresponding to a given current break oscillogram can be obtained by selecting the furnace temperature at which a current make oscillogram displays an equal resistive component.

ELECTRODE-TO-ELECTROLYTE CONTACT RESISTANCE

The existence of appreciable contact resistance between electrode and electrolyte due to the electrode contacting only a small fraction of the electrolyte surface can be detected using

current-make oscillograms and comparing the measured resistance with calculated values based on the sample geometry. The theoretical calculations of Eisenberg and Fick³ on the contact resistance of idealized contacts may be used to estimate the effective area of contact.

EFFECT OF HIGH ELECTRODE RESISTIVITY/THICKNESS PARAMETER

When the electrode resistivity/thickness parameter is less than one, the electrode surface can be considered an equipotential. A uniform current density in the electrolyte between the two electrode can be expected. If high resistance electrodes are tested, the assumption of uniform current density will not hold and care must be used in interpreting tester results. The electrode-to-electrolyte probe will then indicate the resistive and polarization drops associated with the reduced current density existing in the electrolyte near the electrode potential probe. A rough estimate of the actual current density at the probe may be obtained from the resistive component of the current interruption-oscillogram. A back-up current-distribution screen has been used in several experiments to make the electrode surface more nearly an equipotential and to obtain more reliable measurements of polarization.

CONCLUSIONS

An apparatus for the testing of electrode structures for high temperature, solid-electrolyte fuel cells has been described. Independent measurement of electrode resistivity/thickness and resistive and polarization voltage drops corresponding to electrode operation at various current densities (reaction rates), temperatures, and atmospheres have been carried out using current-interruption and current-establishment oscillograms. These techniques have proved useful and are being used in our efforts to develop low cost, long-life electrodes for solid-electrolyte fuel cells.

REFERENCES

1. L. J. van der Pauw, Philips Research Reports, 13, 1, 1958.
2. I. Trachtenberg, J. Electrochem. Soc., 3, 110, 1964.
3. M. Eisenberg and L. Fick, ACS Symposium on Recent Advances in Fuel Cells, 6, 46, 1961.

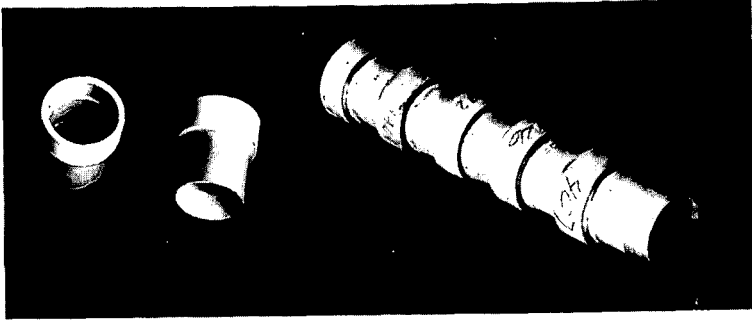


Fig. 1.-Bell-and-spigot fuel cells with five-cell battery assembly

1. Oxygen molecules diffuse through air to electrode surface
2. Adsorption and dissociation of O_2
3. Surface migration to reaction site
4. Oxygen combines with electrons from fuel side of previous cell forming O^{2-} ions
5. Ionic transport of O^{2-} through electrolyte
6. Deionization and surface reaction with fuel, delivery of electrons to the fuel electrode
7. Diffusion of fuel to fuel electrode surface
8. Adsorption of fuel on electrode, surface migration to reaction site.
9. Desorption of reaction product and diffusion into fuel stream

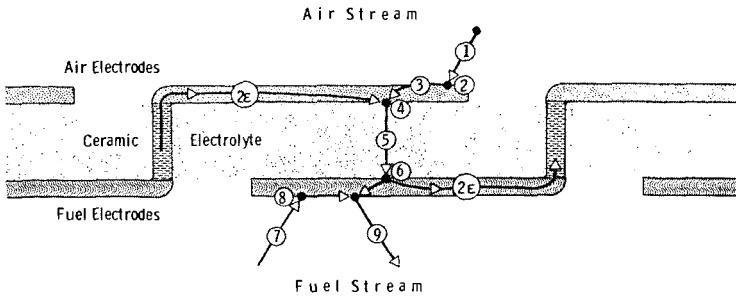
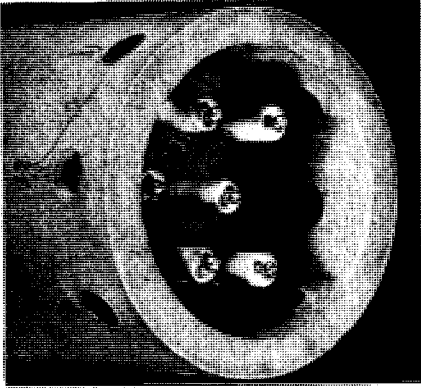
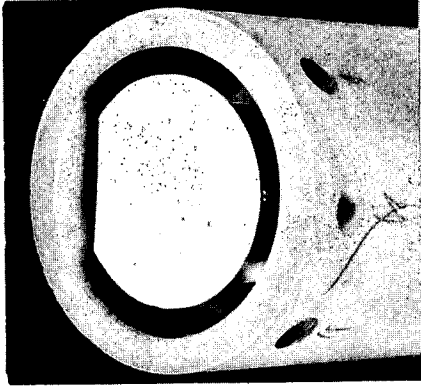


Fig. 2.-An electrode reaction process chain for solid electrolyte fuel cells



Water Cavity in Lava Tube, Showing Probes



Cavity with Electroded Water in Place

Fig. 4.-Internal views of electrode tester

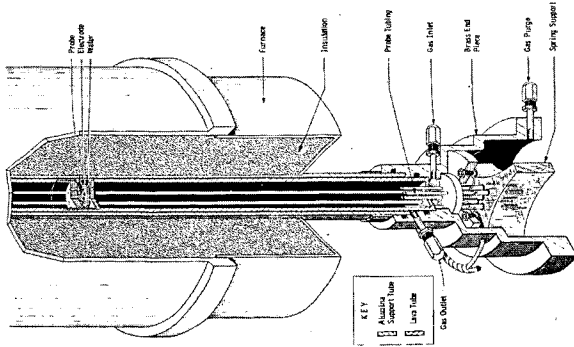


Fig. 3.-Cutaway drawing of electrode tester

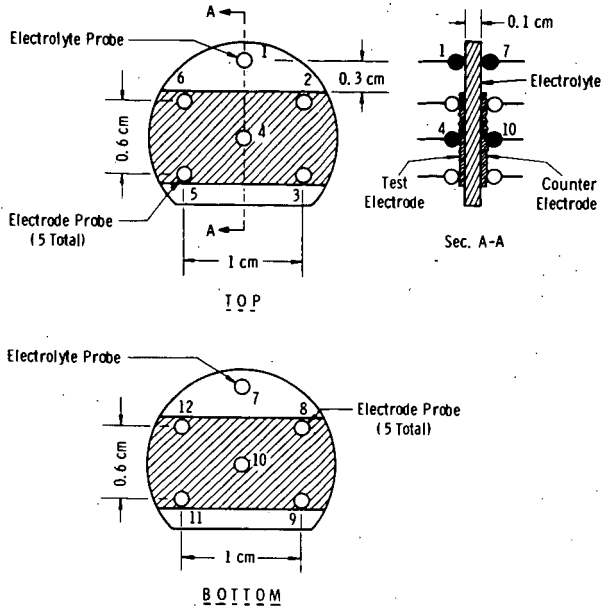


Fig. 5—Probe locations in the electrode tester

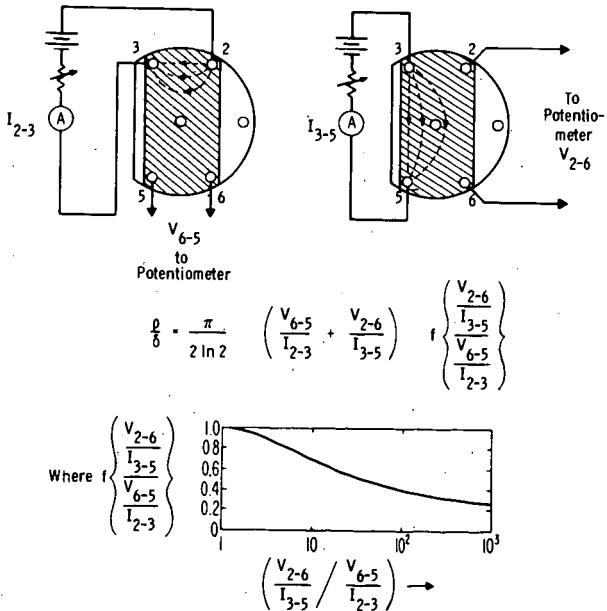


Fig. 6—Measurements to determine the electrode resistivity / thickness parameter using the van der Pauw technique

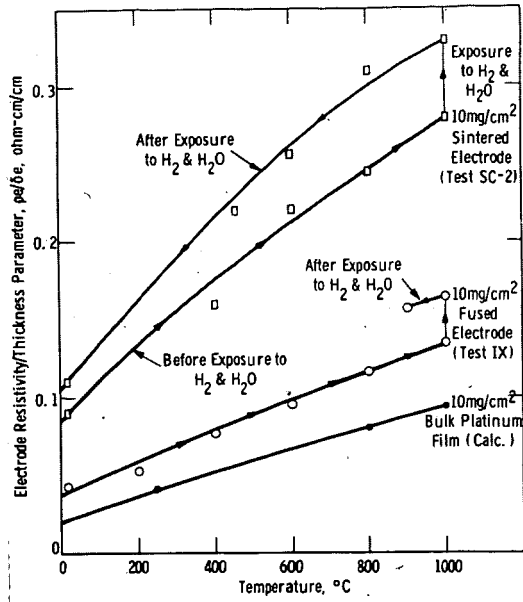
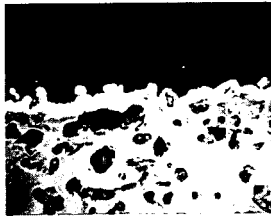
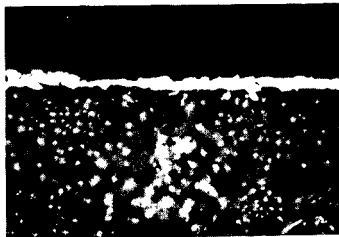


Fig. 7-A comparison of the temperature dependence of the resistivity/thickness parameter, (ρ/δ), for sintered and fused platinum electrodes



Sintered Platinum Electrode: 1000X



Fused Platinum Electrode: 1000X

Fig. 8.-Cross-section photomicrographs of platinum electrodes

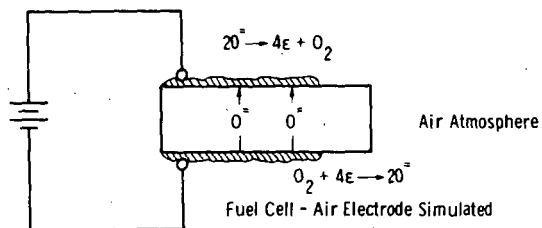
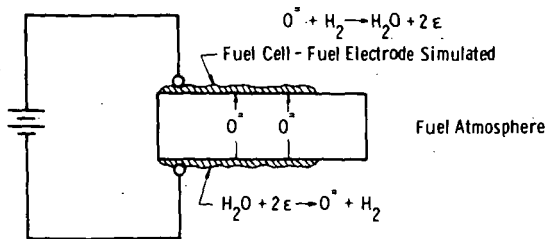


Fig. 9—Simulation of air electrode and fuel electrode operation by choice of current direction and surrounding atmosphere

Dwg. 746A197

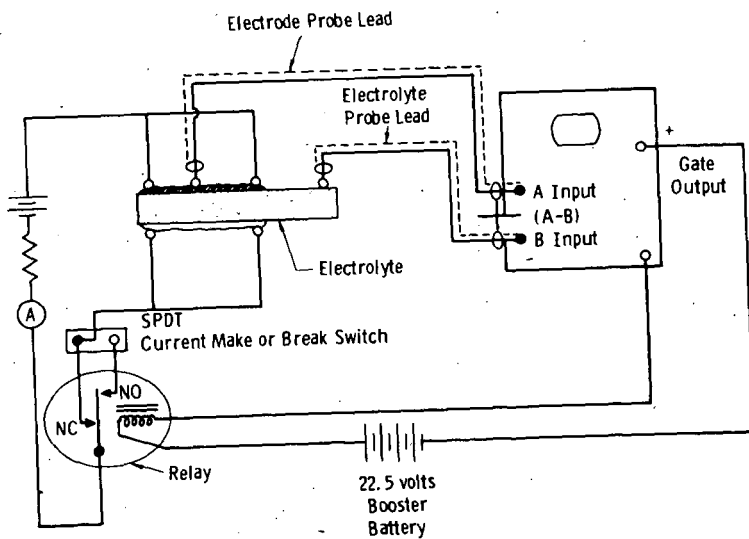
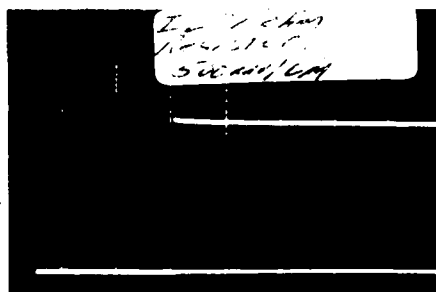
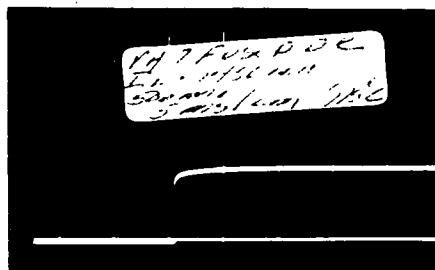


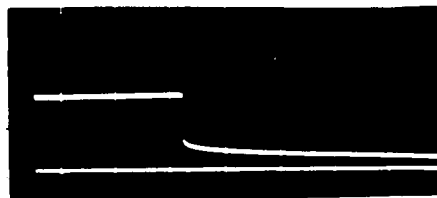
Fig. 10—Circuit used for electrode to electrolyte potential measurements



Sample Current
(Voltage Drop Across
a 1.00 ohm Resistor)



Current Establishment
Oscillogram



Current Break
Oscillogram

Vertical Scale: 500 mv/cm
Horizontal Scale: 5 msec/cm

Fig. 11—Current establishment and current interruption
oscillograms

Fused Platinum Electrode Test XXXIV
H₂ Saturated with H₂O at 26°C 975°C

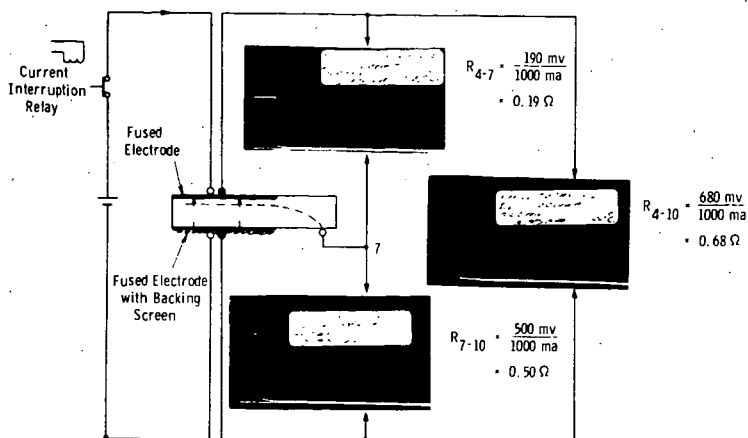


Fig.12—Illustrating method of measuring electrical position of electrolyte potential probe using resistive component from current interruption tests

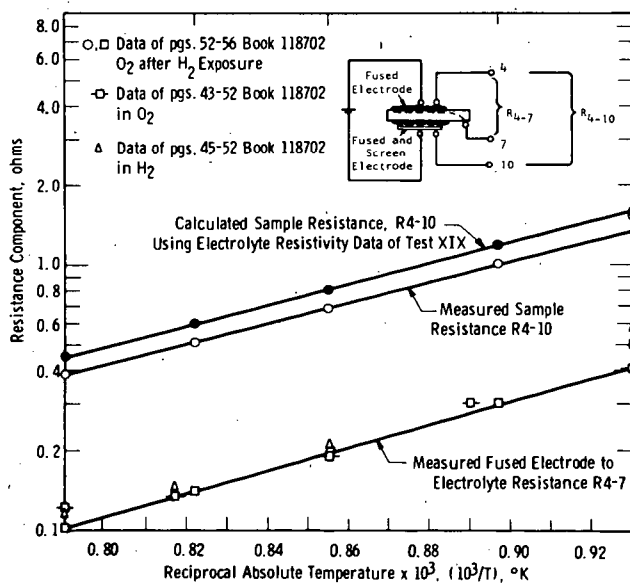
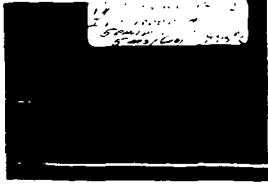
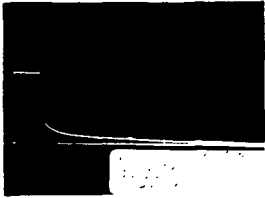


Fig.13—Measurements of the electrical position of the electrolyte potential probe



Fuel electrode performance in oxygen atmosphere
 Vertical scale: 100 mv/cm
 Horizontal Scale: 5 ms/cm
 Indicated R = 0.1 ohms
 Indicated polarization: 0 mv



Fuel electrode performance in hydrogen saturated with water at 70°C
 Vertical scale: 100 mv/cm
 Horizontal scale: 5 ms/cm
 Indicated R = 0.1 ohms
 Indicated polarization: 105 mv

Fig. 14—Electrical performance of fused electrode sample 517 desorbing in oxygen and hydrogen atmospheres
 Test XXXII Test Temp. 995°C
 Sample current 1.0 amperes
 Electrode current density 740 ma/cm²

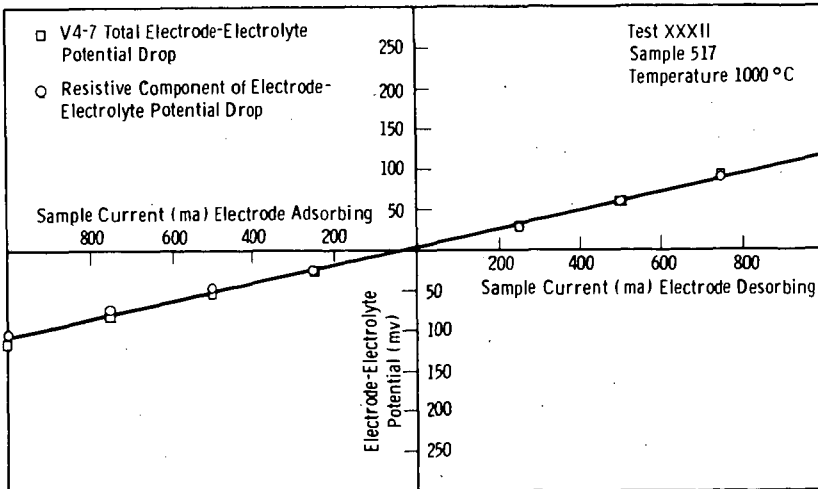


Fig. 15—Volt-ampere characteristic of fused electrode in an oxygen atmosphere

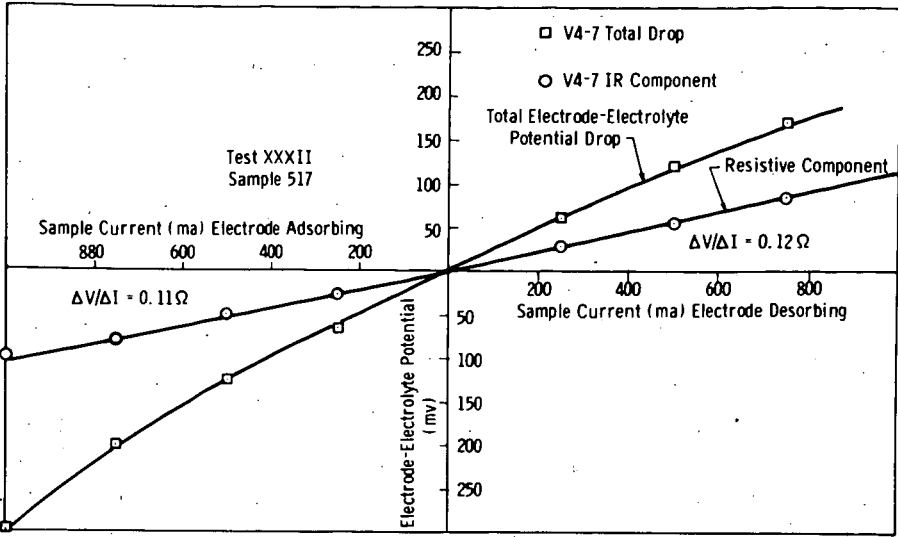


Fig. 16-Volt-ampere characteristic of fused electrode in H_2 and H_2O atmosphere at $1000^\circ C$

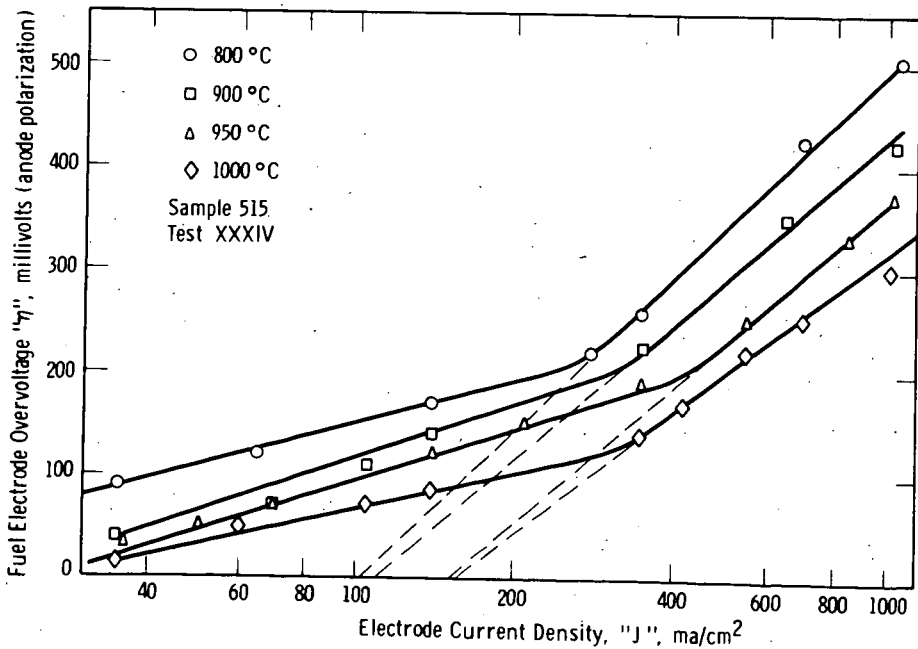


Fig. 17-Fuel electrode polarization as a function of electrolyte temperature